Journal of Hazardous Materials 187 (2011) 466–472

Contents lists available at ScienceDirect

Journal of Hazardous Materials

journal homepage: www.elsevier.com/locate/jhazmat

Facile synthesis of Ag nanoparticles supported on MWCNTs with favorable stability and their bactericidal properties

Zhenzi Li, Lijun Fan, Tao Zhang, Kang Li*

Department of Epidemiology and Biostatistics, Harbin Medical University, Harbin 150086, People's Republic of China

ARTICLE INFO

Article history:
Received 27 September 2010
Received in revised form 12 January 2011
Accepted 12 January 2011
Available online 18 January 2011

Keywords:
Ag nanoparticle
Multi-walled carbon nanotube
Bactericidal property
Favorable stability
Escherichia coli

ABSTRACT

Stable Ag nanoparticles supported on multi-walled carbon nanotubes (MWCNTs) have been successfully synthesized by calcinations of the complexes of Ag cation and acid-treated MWCNTs under sparging N_2. The nanocomposites are characterized in detail by X-ray diffraction (XRD), scanning electron microscopy (SEM), transmission electron microscopy (TEM) and UV–visible absorption spectroscopy. The results indicate that Ag nanoparticles are relatively homogeneously dispersed on the surface of MWCNTs. The bactericidal properties of Ag/MWCNT nanocomposites are investigated with disk diffusion assay on the suspension samples inoculated with *Escherichia coli*. The results show that Ag/MWCNTs-500 nanocomposites possess excellent bactericidal property because of their suitable particle size (15 nm). Moreover, Ag nanoparticles supported on MWCNTs are very stable for half a year. What is more, the bactericidal effect was enhanced obviously under solar irradiation. This is because MWCNTs can absorb near-infrared light to kill parts of bacteria. A possible formation mechanism is also proposed in this article.

1. Introduction

Ag nanoparticles have been extensively investigated in the fields of optical and electro-optical devices, catalyst, surface-enhanced Raman spectroscopy substrate, and bactericidal [1–8]. It is well-known that the high surface energy of the Ag nanoparticles makes them reactive and apts to be oxidized under air, could easily aggregate to big particles and lose their characteristics. Therefore, the stability is one of the most important factors for their practical applications in nanoscience and nanotechnology [9,10]. In general, there are two types of methods for stabilizing Ag nanoparticles. One is to employ organic molecules to prevent the aggregation and oxidation of the Ag nanoparticles [11–13]. In this system, the small water-soluble organic molecules can be used to protect Ag nanoparticles in aqueous solution conveniently but only with low yields and low stability. The other is to deposit Ag nanoparticles on host materials for fabricating nanocomposites. These hybrid materials have many advantages over conductivity, catalytic activity as well as in biochemistry for the potential application such as chemical sensors [14,15]. Moreover, the assembly of metal nanoparticles on the support could enhance their stability and easy separation from the reaction medium for recycle. The usually used host materials are SiO_2, zeolite, and carbon materials [16–18]. Among them, carbon materials have been considered to be the excellent supporters because of their predominant properties and biocompatibility.

Carbon nanotubes (CNTs) with unique nanostructures have attracted much attention due to their remarkable electronic and mechanical properties, thermal stability and high aspect ratio [19]. However, owing to the high aspect ratio and the strong van der Waals attraction between the CNTs, the raw CNTs tend to aggregate into a dense and robust network of ropes, resulting in poor solubility [20]. In order to extend their potential applications in biomedicine and biotechnology, extensive research has been focused on the surface modification of CNTs mainly to enhance their chemical compatibility and dispersibility [21–24]. Multi-walled carbon nanotubes (MWCNTs) are more commonly used because of their low cost compared with single-walled carbon nanotubes (SWCNTs) [25]. Moreover, MWCNTs are made of concentric cylinders placed around a common central hollow, with spacing between the layers close to that of the interlayer distance in graphite (0.34 nm) [26]. Therefore, MWCNTs would be more complicated than that of SWCNTs, to some extent. The raw MWCNTs are usually long, tangled together and have closed ends, which will increase the bulk viscosity of CNT-based materials. This phenomenon will limit the application of MWCNTs. Therefore, in order to solve these problems, it is very important to obtain the short and functionalized MWCNTs. Functionalization of the pristine MWCNTs in nitric acid will result in the presence of carboxylic acid groups (–COOH) on the surface of MWCNTs, where the raw MWCNTs were shortened and debundled simultaneously [27–29]. Furthermore, the short and functionalized MWCNTs resulted in the increase of

* Corresponding author at: Xuefu Road 194, Nangang District, Harbin, People's Republic of China. Tel.: +86 451 8750 2939; fax: +86 451 8750 2831.
E-mail address: Likang@ems.hrbmu.edu.cn (K. Li).

0304-3894/$ – see front matter © 2011 Elsevier B.V. All rights reserved.
doi:10.1016/j.jhazmat.2011.01.050

defects and surface area, which makes it possible to couple other materials on the MWCNTs [30–33]. Defects are therefore a promising starting point for further application of MWCNTs.

On the basis of the above consideration, in this article, utilizing the acid-treated MWCNTs as the supporter, we prepared Ag/MWCNTs nanocomposites with favorable stability. The acid-treated MWCNTs possess abundant functional groups such as –COOH and can form complexes with Ag ions in diluted solutions. Experimental results showed that Ag/MWCNT nanocomposites were successfully synthesized after calcination under sparging N_2. Ag nanoparticles were relatively homogeneously dispersed on the surface of MWCNTs. The bactericidal properties of Ag/MWCNTs nanocomposites were examined with disk diffusion assay on the suspension samples inoculated with *Escherichia coli*, which usually existed in fecal pollution waters and could cause a typical infection to human body, and the results showed that the composites possessed excellent bactericidal properties. Furthermore, Ag nanoparticles were very stable even after several months. The simple, environmental friendly and cost-effective nanocomposites may have more promising applications in nanoscience and nanotechnology.

2. Materials and methods

2.1. Materials

All chemical reagents were obtained from commercial source as guarantee-graded reagents and used without further purification. MWCNTs and *E. coli* were purchased from Shenzhen Nanotech. Port. Co. and Fisher Company, respectively.

2.2. Acid treatment of MWCNTs

In a typical procedure [34], 1 g raw MWCNTs were suspended in 40 mL concentrated nitric acid and sonicated for 0.5 h. The mixture was refluxed at 140 °C for 14 h under vigorous stirring. And then, the MWCNTs were collected on filter paper and washed with deionized water until pH = 7. Finally, the functionalized MWCNTs were dried under vacuum at 50 °C overnight.

2.3. Preparation of Ag/MWCNTs nanocomposites

Typically, 20 mg MWCNTs were added to 10 ml aqueous solution (0.1 M) of the $AgNO_3$, and then sonicated for 1 h, aged overnight to obtain Ag^+/MWCNTs complexes. The Ag^+/MWCNTs complexes were then washed by deionized water followed by vacuum drying at 50 °C for 24 h. Subsequently, the complexes were placed in a quartz boat and heated to a final temperature (400, 500, 600, and 800 °C) for 1 h under sparging N_2 at a rate of 5 °C min^{-1} in a horizontal tube furnace. After cooling to room temperature, black products were obtained. The corresponding samples were denoted as Ag/MWCNTs-400, Ag/MWCNTs-500, Ag/MWCNTs-600, Ag/MWCNTs-800, respectively.

2.4. Characterization

X-ray diffraction (XRD) patterns were obtained by a Rigaku D/max-IIIB diffractometer using Cu Kα radiation (λ = 1.5406 Å). Scanning electron microscopy (SEM) micrographs were taken using a Hitachi S-4300 instrument equipped with an Energy Dispersive X-ray (EDX) detector operating at 20 kV. Transmission electron microscopy (TEM) experiment was performed on a JEM-3010 electron microscope (JEOL, Japan) with an acceleration voltage of 300 kV. Carbon-coated copper grids were used as the sample holders. UV–visible absorption spectra were obtained using UV-visible spectrophotometer (UV-5520). Fourier transform infrared (FT-IR) spectra were recorded on a PerkinElmer Spectrum One spectrometer using KBr pellets. X-ray photoelectron spectroscopy (XPS) measures were performed with AXIS UL TRA DLD.

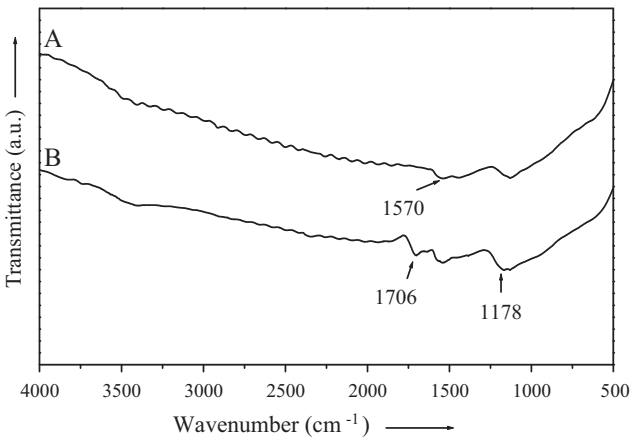

Fig. 1. FT-IR spectra of raw MWCNTs (A) and acid-treated MWCNTs (B).

2.5. Evaluation of bactericidal activity

Bactericidal activity of Ag/MWCNT nanocomposites were tested on *E. coli* by the standard disk diffusion assay on LB agar medium: a solid form of medium used to create plates for streaking out bacterial colonies. All glassware and materials were sterilized in autoclave at 120 °C for 0.5 h before experiments. The disk diffusion assay was performed by placing a 10 mm filter paper treated with 20 μL of Ag/MWCNT nanocomposites aqueous slurry (100 μg μL^{-1}) onto an agar plate seeded with approximately 10^7 colony forming units (CFU) of *E. coli*. After incubation at 37 °C one day, the diameters of the inhibition zones were observed and measured. Control experiments (absence of Ag/MWCNT nanocomposites) were made to check for the growth of the *E. coli*. Minimum bactericidal concentration (MBC) of commonly used antibiotics (Streptomycin) was determined to compare the effect ion of the Ag/MWCNTs nanocomposites. Meanwhile, samples with solar irradiation from 10 a.m. to 4 p.m. (temperature range 36 ± 1 °C) for 6 h were also performed to investigate the effect of solar light.

3. Results and discussion

3.1. FT-IR and XPS analysis

The presence of carboxylic acid groups on the surface of MWCNTs can offer opportunity to form complexes with different metal cations. Therefore, in order to obtain Ag/MWCNTs nanocomposites, we should confirm the presence of –COOH on MWCNTs firstly. The FT-IR spectra of the raw MWCNTs and acid-treated MWCNT are shown in Fig. 1A and B, respectively. As shown in Fig. 1A, the raw MWCNTs clearly present a FT-IR peak centered at 1570 cm^{-1}, which can be assigned to the C=C stretching of carbon nanotube backbones [35,36]. As for acid-treated MWCNTs (Fig. 1B), the characteristic absorption peaks indexed as C=O and C–O stretching bands are clearly visible at 1706 and 1178 cm^{-1}, respectively, which are the typical bands of carboxylic acid groups [36–38]. FT-IR results demonstrate that the MWCNTs have been successfully decorated with carboxylic acid groups. Carboxylic acid groups on the sidewalls are very important for the MWCNTs because these groups can act as anchor groups to couple with other materials.

In order to further confirm the existence of these carboxylic acid groups, surface characterization of XPS was made. Fig. 2 shows the XPS plots of the C 1s core levels of raw MWCNTs and acid-treated

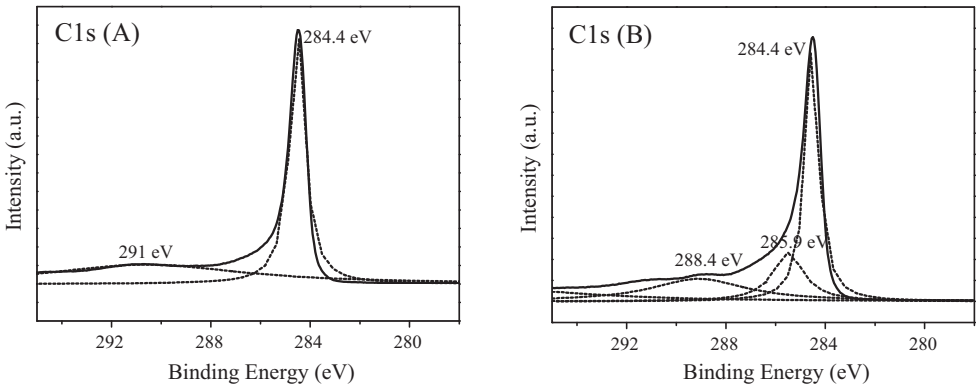

Fig. 2. XPS plots of the C 1s core levels of raw MWCNTs (A) and acid-treated MWCNTs (B).

MWCNTs. The C 1s spectral region of raw MWCNTs shows two binding energy (BE) peaks. The C 1s peak at BE = 284.4 eV is due to the underlying MWCNTs graphene sheets (Fig. 2A), which did not undergo being functionalized with carboxylic acid groups [39]. Moreover, the C 1s peak at BE = 291 eV could be attributed to alkyl carbons on the graphene sheet [39]. It is very interesting to note that the C 1s spectral region of the acid-treated MWCNTs (Fig. 2B) shows two main oxidation states at 285.9 and 288.4 eV, denoting –C–O– and –COOH tethered to the MWCNTs, respectively [39–41]. These results illustrated that certain amounts of carboxylic acid groups indeed existed on the surface of acid-treated MWCNTs. This is consistent with the FT-IR result.

3.2. XRD analysis

The structure and chemical composition of the resultant Ag/MWCNTs nanocomposites synthesized in this study were confirmed by XRD and the results are shown in Fig. 3. From Fig. 3b–e, four high-intensity diffraction peaks at $2\theta = 37.7$, 44.0, 64.2, and 79° can be observed, which can be indexed as (1 1 1), (2 0 0), (2 2 0), and (3 1 1) diffraction for Ag (JCPDS (Joint Committee on Powder Diffraction Standards) No. 04-0783), respectively. At the same time, all samples feature one Bragg diffraction peak at about 26° (2θ), which is the characteristic of carbon nanotubes (Fig. 3) [42]. The XRD results showed that the composites were composed of Ag and MWCNTs. Furthermore, the effect of calcination temperature on the final structure was also investigated and found that the crystalline size increased obviously with the increase of calcination temperature. The crystalline size of Ag nanoparticles was determined from Scherrer equation using the (1 1 1) diffraction peak of the samples calcined at 400, 500, 600 and 800 °C, the average crystalline size was found to be 12, 15, 19 and 23 nm, respectively. A similar result was also found for the (2 0 0) diffraction peak.

3.3. UV–vis absorption

UV–vis absorption spectroscopy has been proved to be a suitable and effective method for evaluating the aggregation of Ag nanoparticles. The UV–vis spectra of Ag/MWCNT nanocomposites are shown in Fig. 4. We can clearly see that only one absorption band is observed in the range between 300 and 900 nm for these four samples. A maximum absorption peak (λ_{max}) at 410 nm of Ag/MWCNTs-400 was presented, which was the characteristic of Ag nanoparticles [43–45]. With the increase of calcination temperature, the position of absorption peak was gradually red-shifted. The λ_{max} of Ag/MWCNTs-800 nanocomposites was 431 nm, which was a 21 nm red-shift compared with Ag/MWCNTs-400 nanocomposites. The red-shift of the λ_{max} is mainly because the Ag particles grow larger as the calcination temperature increased [46]. On the other hand, we can also see that the absorption band was broad, which may be resulted from the plasmon–plasmon interaction between the adjacent Ag nanoparticles [47].

3.4. SEM–EDX analysis

The morphology of Ag/MWCNTs nanocomposites was performed by SEM. The typical SEM image of Ag/MWCNTs-500 nanocomposites is shown in Fig. 5A. We can clearly see that Ag nanoparticles with uniform diameter were covered on the surface of MWCNTs relatively homogeneously. Fig. 5B shows the EDX

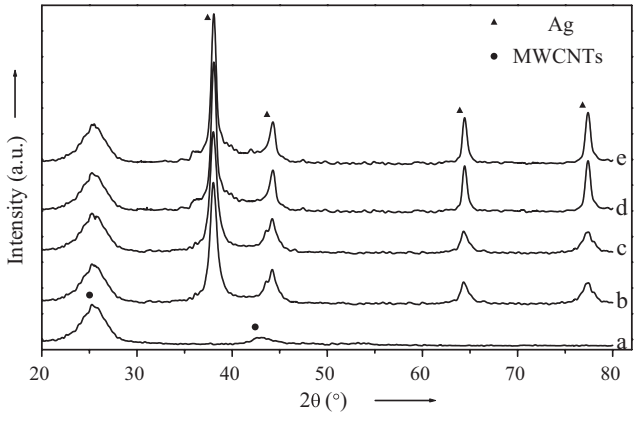

Fig. 3. XRD patterns of MWCNTs (a), Ag/MWCNTs-400 (b), Ag/MWCNTs-500 (c), Ag/MWCNTs-600 (d), and Ag/MWCNTs-800 nanocomposites (e).

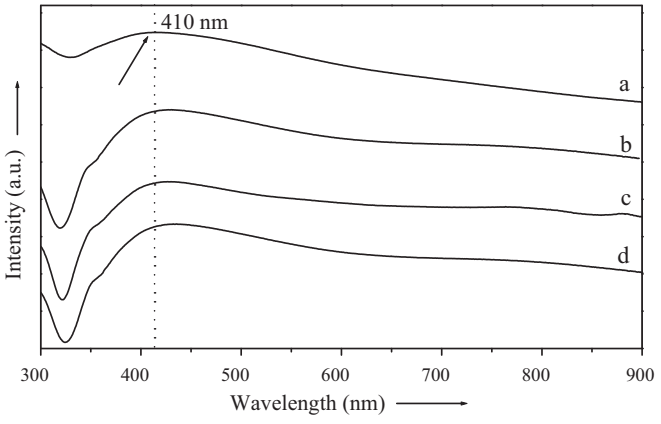

Fig. 4. UV–vis spectra of Ag/MWCNTs-400 (a), Ag/MWCNTs-500 (b), Ag/MWCNTs-600 (c), and Ag/MWCNTs-800 nanocomposites (d), respectively.

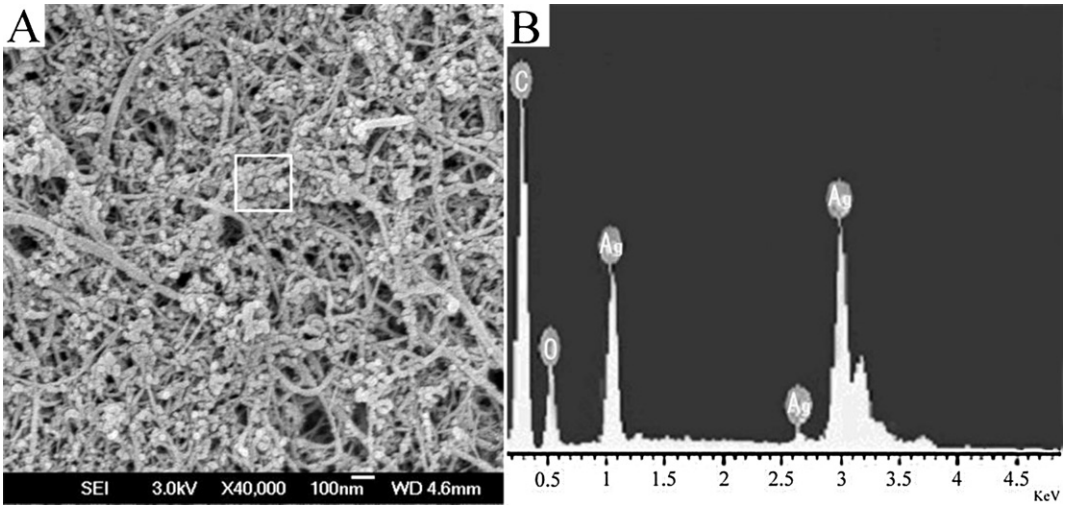

Fig. 5. The SEM image of Ag/MWCNTs-500 nanocomposites (A) and its corresponding EDX spectrum (B).

spectrum of the defined area of Ag/MWCNTs nanocomposites. The characteristic peaks of Ag and MWCNTs were clearly observed, indicating the existence of Ag and MWCNTs. This is in agreement very well with XRD results. The content of Ag element was over 90% in quality, suggesting that Ag nanoparticles were indeed existed in the composite.

3.5. Morphology observation

The typical TEM image of Ag/MWCNTs-500 nanocomposites is shown in Fig. 6. Obviously, Ag nanoparticles (marked with arrows) with the main diameter around 15 nm were well dispersed on the surface of MWCNTs. This confirms the fact that Ag/MWCNT nanocomposites were formed and Ag nanoparticles were relatively homogeneously dispersed on the surface of MWCNTs. On one hand, MWCNTs acted as supporters for Ag nanoparticles. On the other hand, MWCNTs were excellent disperser which inhibited the aggregation of Ag nanoparticles. Therefore, MWCNTs were one of the best choices for supporting and stabilizing Ag nanoparticles. The TEM observation was consistent very well with the SEM results.

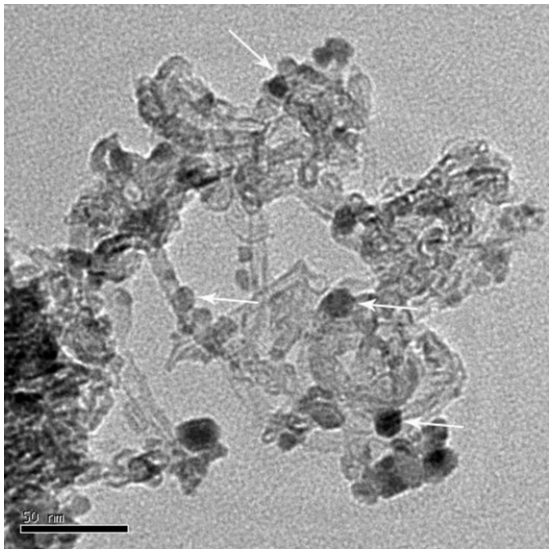

Fig. 6. The TEM image of Ag/MWCNTs-500 nanocomposites.

3.6. Formation mechanism

The above experimental results demonstrate that Ag/MWCNTs nanocomposites have been successfully synthesized through attachment of Ag nanoparticles onto the surface of acid-treated MWCNTs. Schematic depiction of the reasonable formation mechanism of Ag/MWCNT nanocomposites is shown in Scheme 1. It is well-known that the raw MWCNTs tend to aggregate into a dense and robust network of ropes because of their high aspect ratio and the strong van der Waals attraction between the MWCNTs, resulting in their poor solubility in most solvents [20]. Therefore, the practical application is limited greatly. In order to extend their application, the treatment of concentrated HNO_3 is adopted. After refluxing in concentrated HNO_3, –COOH is present on the surface of MWCNTs, mainly located on the defects of MWCNTs. Then acid-treated MWCNTs are added to the aqueous solution of $AgNO_3$. After sonication, MWCNTs are homogeneously dispersed in the solution. Meanwhile, Ag cation with positive charge can interact with –COOH of MWCNTs which has negative charge through electrostatic interaction. After calcination under N_2 protection, Ag nanoparticles are attached on the surface of MWCNTs firmly. Ag/MWCNTs nanocomposites are formed ultimately.

3.7. Bactericidal property

Ag nanoparticles have proved to have strong inhibitory and bactericidal effect [3,48]. Many Ag composites have been used as bactericidal materials [49–51]. However, they were not widely applied in practical applications because of their low stability and high cost. In this article, bactericidal activities of Ag/MWCNT nanocomposites against *E. coli* were evaluated by determining the presence of inhibition zones. At first, the amount of Ag supported on the surface of MWCNT was investigated by changing the mass ratio of Ag and MWCNT. We controlled the mass ratio of Ag and MWCNT for 1:1, 3:1, 5:1, 7:1 and 10:1, respectively. As for the mass ratio of 1:1, the amount Ag on the surface of MWCNTs was little, so the bactericidal performance was poor. However, if we increased the mass ratio of Ag and MWCNTs up to 10:1, many Ag nanoparticles aggregated into big particles, because acid-treated MWCNT could not offer so much –COOH sites. Therefore, the bactericidal performance was poor as well. Based on these above facts, the mass ratio of 5:1 was the best choice for better bactericidal effect. Fig. 7 shows the bactericidal effects in the form of inhibition zones, which was assessed by the disk diffusion assay of the Ag/MWCNTs nanocom-

Scheme 1. Schematic depiction of the reasonable formation mechanism of Ag/MWCNTs nanocomposites.

Table 1
The inhibitory effect for different samples.

Samples	Inhibition zone (fresh[a]) (mm)	Inhibition zone (old[b]) (mm)
Blank	0	–
Ag/MWCNTs-400	25.9	25.2
Ag/MWCNTs-500	26.8	26.3
Ag/MWCNTs-600	24.1	23.8
Ag/MWCNTs-800	23.8	23.1
Streptomycin	26.7	–

[a] The inhibition zone of the fresh obtained samples.
[b] The inhibition zone of the obtained samples after storing for half a year at room temperature.

posites for the mass ratio of 5:1. As a control, experiment of pure water without any Ag/MWCNT nanocomposites was made (Fig. 6A). The picture of inhibition zones was not observed, and it implied that the effect of water could be ignored. We can clearly see that Ag/MWCNTs nanocomposites possessed bactericidal activity from Fig. 7B–E. The details of experimental data of bactericidal effect for different samples are listed in Table 1. The diameters of inhibition zone for Ag/MWCNTs-400, Ag/MWCNTs-500, Ag/MWCNTs-600, and Ag/MWCNTs-800 nanocomposites were 25.9, 26.8, 24.1, and 23.8 mm, respectively. Among them, Ag/MWCNTs-500 nanocomposites possessed the best bactericidal activity. Moreover, in this study, Streptomycin was selected as the standard bactericidal material and the inhibition zone was up to 26.7 mm (Fig. 7F). Compared with Streptomycin, Ag/MWCNTs-500 nanocomposites had similar excellent bactericidal effect. It is very interesting to note that the bactericidal activities of Ag/MWCNT nanocomposites increased first, and then decreased with the increase of calcination temperature. With the increase of temperature, the Ag nanoparticles gradually grew into bigger nanoparticles. At the temperature of 500 °C, the size of Ag nanoparticles (15 nm) was best for bactericidal property. The Ag nanoparticles were gradually aggregated into big particles and thus decreased the efficient surface area with further increase in the temperature. Therefore, the bactericidal activities decreased when the calcination temperature was higher than 500 °C. In case of the above results, we can confirm that the difference of the bactericidal properties for different samples was due to the size (as shown in the part of XRD analysis) variety of Ag nanoparticles.

Stability is an important factor for Ag nanocomposites in practical applications. In our study, the stability of Ag/MWCNTs nanocomposites was also investigated. In order to testify the composition of Ag/MWCNTs nanocomposites after storing for half a year at room temperature, XRD measurements were performed (data shown in Supplementary Data, Fig. S1,). The XRD patterns of all samples were almost the same compared with the fresh samples shown in Fig. 3. This confirmed that the structure and composition

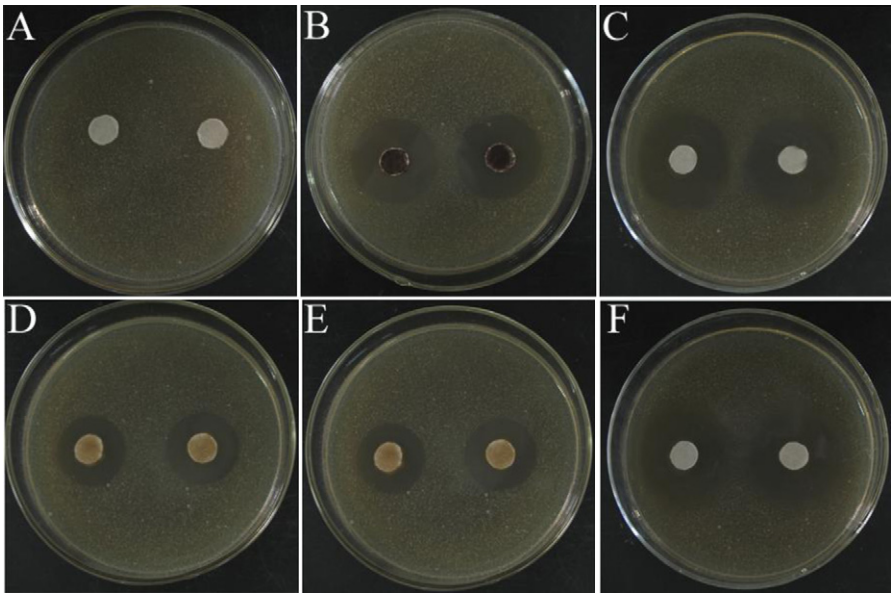

Fig. 7. Comparison of the inhibition zone test among the control used pure water (A), Ag/MWCNTs-400 (B), Ag/MWCNTs-500 (C), Ag/MWCNTs-600 (D), Ag/MWCNTs-800 nanocomposites (E) and Streptomycin (F).

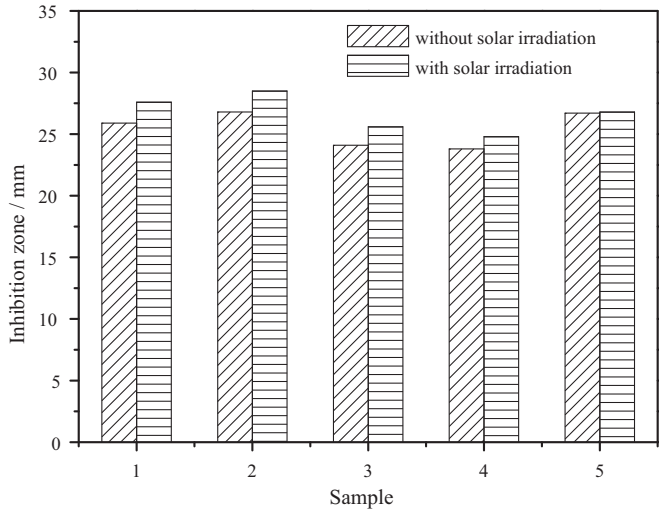

Fig. 8. The inhibition zone of the fresh obtained samples with and without solar irradiation for one day. (1: Ag/MWCNTs-400, 2: Ag/MWCNTs-500, 3: Ag/MWCNTs-600, 4: Ag/MWCNTs-800 and 5: Streptomycin).

of Ag/MWCNTs nanocomposites was not changed, that was to say, the nanocomposites were very stable. In addition, the bactericidal activity of all samples was evaluated once again. The inhibition zones of the samples stored for half a year are shown in Table 1. We can clearly see that inhibition zones of all samples were almost invariably with that of fresh samples. The XRD and bactericidal study indicated that Ag nanoparticles supported on MWCNTs were very stable and they did not change obviously even after half a year. The high stability of Ag/MWCNTs nanocomposites maybe due to the interaction between Ag nanoparticles and MWCNTs, and the passivate effect of MWCNTs for Ag nanoparticles.

Solar energy is clean, huge and convenient. Therefore, if it can be used to sterilize under certain conditions, it will have more potential applications in the future. In order to investigate the effect of solar irradiation, the samples were irradiated under solar for one day ($36 \pm 1\,^{\circ}C$). The inhibition zone of the fresh obtained samples with and without solar irradiation is shown in Fig. 8. It is very interesting to note that bactericidal effect for different samples is enhanced obviously under solar irradiation. However, the bactericidal effect of Streptomycin is nearly the same with and without solar irradiation. This is because MWCNTs possess the characteristics of the absorption of near-infrared [52–54]. Under solar irradiation, the energy that MWCNTs absorbed and stored near-infrared light may be kill parts of bacteria. Therefore, under solar irradiation, the bactericidal effect was enhanced. Moreover, visible light from the solar irradiation could lead to plasmon resonance of Ag nanoparticles, which is confirmed as a visible light photocatalyst [55]. And this visible light photocatalyst could kill parts of bacteria as well. Therefore, the enhanced bactericidal activity could be ascribed to the synergistic effect of two factors mentioned above. Therefore, this facile and economical method utilizing the solar energy would have good potential in bactericidal applications.

4. Conclusions

In summary, Ag/MWCNT nanocomposites have been successfully synthesized by a simple method. The results confirmed that Ag nanoparticles supported on the surface of MWCNTs relatively homogeneously. The bactericidal activities showed that Ag/MWCNTs-500 nanocomposites possessed the most excellent bactericidal properties compared with other samples, which had suitable particle size (15 nm). Ag nanoparticles in this sample were very stable for half a year because of the interaction between Ag nanoparticles and MWCNTs and the passivate effect of MWCNTs for Ag nanoparticles. Furthermore, the bactericidal effect was enhanced obviously under solar irradiation due to the synergistic effect of MWCNTs possess the absorption performance of near-infrared and Ag nanoparticles possess visible light photocatalytic activity. This facile and green approach can be extended to synthesize other composite materials and may have more promising applications in nanoscience.

Acknowledgment

This work was supported by the National Natural Science Foundation of China (No. 30872185).

Appendix A. Supplementary data

Supplementary data associated with this article can be found, in the online version, at doi:10.1016/j.jhazmat.2011.01.050.

References

[1] L.N. Lewis, Chemical catalysis by colloids and clusters, Chem. Rev. 93 (1993) 2693–2730.
[2] V. Alt, T. Bechert, P. Steinrucke, M. Wagener, P. Seidel, E. Dingeldein, E. Domann, R. Schnettler, An in vitro assessment of the antibacterial properties and cytotoxicity of nanoparticulate silver bone cement, Biomaterials 25 (2004) 4383–4391.
[3] A. Melaiye, Z. Sun, K. Hindi, A. Milsted, D. Ely, D.H. Reneker, C.A. Tessier, W.J. Youngs, Silver(I)-imidazole cyclophane gem-diol complexes encapsulated by electrospun tecophilic nanofibers: formation of nanosilver particles and antimicrobial activity, J. Am. Chem. Soc. 127 (2005) 2285–2291.
[4] C. Aymonier, U. Schlotterbeck, L. Antonietti, P. Zacharias, R. Thomann, J.C. Tiller, S. Mecking, Hybrids of silver nanoparticles with amphiphilic hyperbranched macromolecules exhibiting antimicrobial properties, Chem. Commun. 24 (2002) 3018–3019.
[5] J.R. Morones, J.L. Elechiguerra, A. Camacho, K. Holt, J.B. Kouri, J.T. Ramírez, M.J. Yacaman, The bactericidal effect of silver nanoparticles, Nanotechnology 16 (2005) 2346–2353.
[6] S. Nie, S.R. Emory, Probing single molecules and single nanoparticles by surface-enhanced Raman scattering, Science 275 (1997) 1102–1106.
[7] L. Lu, H. Wang, Y. Zhou, S. Xi, H. Zhang, J. Hu, B. Zhao, Redox-active two-dimensional coordination polymer: preparation of silver and gold nanoparticles and crystal dynamics on guest removal, Chem. Commun. 1 (2002) 144–145.
[8] C.N. Lok, C.M. Ho, R. Chen, Q.Y. He, W.Y. Yu, H. Sun, P.K.H. am, J.F. Chiu, C.M. Che, Proteomic analysis of the mode of antibacterial action of silver nanoparticles, J. Proteome Res. 5 (2006) 916–924.
[9] P. Mulvaney, T. Linnert, A. Henglein, Surface chemistry of colloidal silver in aqueous solution: observations on chemisorption and reactivity, J. Phys. Chem. 95 (1991) 7843–7846.
[10] A. Henglein, Colloidal silver nanoparticles: photochemical preparation and interaction with O_2, CCl_4, and some metal ions, Chem. Mater. 10 (1998) 444–450.
[11] X. Sun, S. Dong, E. Wang, High-yield synthesis of large single-crystalline gold nanoplates through a polyamine process, Langmuir 21 (2005) 4710–4712.
[12] Y. Sun, Y. Xia, Shape-controlled synthesis of gold and silver nanoparticles, Science 298 (2002) 2176–2179.
[13] C.J. Murphy, T.K. Sau, A.M. Gole, C.J. Orendorff, L. Gao, L. Gou, S.E. Hunyadi, T. Li, Anisotropic metal nanoparticles: synthesis, assembly, and optical applications, J. Phys. Chem. B 109 (2005) 13857–13870.
[14] R. Babua, J. Zhang, E.J. Beckmanb, M. Virjia, W.A. Pascullea, A. Wells, Antimicrobial activities of silver used as a polymerization catalyst for a wound-healing matrix, Biomaterials 27 (2006) 4304–4314.
[15] Y.C. Chung, I.H. Chen, C.J. Chen, The surface modification of silver nanoparticles by phosphoryl disulfides for improved biocompatibility and intracellular uptake, Biomaterials 29 (2008) 1807–1816.
[16] Y.H. Zhang, F. Chen, J.H. Zhuang, Y. Tang, D.J. Wang, Y.J. Wang, A.G. Dong, N. Ren, Synthesis of silver nanoparticles via electrochemical reduction on compact zeolite film modified electrodes, Chem. Commun. 23 (2002) 2814–2815.
[17] H. Ortiz-Ibarra, N. Casillas, V. Soto, M. Barcena-Soto, R. Torres-Vitela, W. Cruz, S. Gómez-Salazar, Surface characterization of electrodeposited silver on activated carbon for bactericidal purposes, J. Colloid Interface Sci. 314 (2007) 562–571.
[18] A. Niu, Y. Han, J. Wu, N. Yu, Q. Xu, Synthesis of one-dimensional carbon nanomaterials wrapped by silver nanoparticles and their antibacterial behavior, J. Phys. Chem. C 114 (2010) 12728–12735.
[19] S. Iijima, Helical microtubules of graphitic carbon, Nature 354 (1991) 56–58.
[20] D. Tasis, N. Tagmatarchis, A. Bianco, M. Prato, Chemistry of carbon nanotubes, Chem. Rev. 106 (2006) 1105–1136.
[21] K. Kostarelos, L. Lacerda, G. Pastorin, W. Wu, S. Wieckowski, J. Luangsivilay, S. Godefroy, D. Pantarotto, J.P. Briand, S. Muller, M. Prato, A. Bianco, Cellular

uptake of functionalized carbon nanotubes is independent of functional group and cell type, Nat. Nanotechnol. 2 (2006) 108–113.
[22] S. Banerjee, T. Hemraj-Benny, S.S. Wong, Covalent surface chemistry of single-walled carbon nanotubes, Adv. Mater. 17 (2005) 17–29.
[23] Y. Maniwa, K. Matsuda, H. Kyakuno, S. Ogasawara, T. Hibi, H. Kadowaki, S. Suzuki, Y. Achiba, H. Kataura, Water-filled single-wall carbon nanotubes as molecular nanovalves, Nat. Mater. 6 (2007) 135–141.
[24] D.A. Britz, A.N. Khlobystov, Noncovalent interactions of molecules with single walled carbon nanotubes, Chem. Soc. Rev. 35 (2006) 637–659.
[25] M.D. Lai, J. Li, J. Yang, J.J. Liu, X. Tong, H.M. Cheng, The morphology and thermal properties of multi-walled carbon nanotube and poly (hydroxybutyrate-co-hydroxyvalerate) composite, Polym. Int. 53 (2004) 1479–1484.
[26] P.M. Ajayan, Nanotubes from carbon, Chem. Rev. 99 (1999) 1787–1800.
[27] Y. Xu, C. Gao, H. Kong, D.Y. Yan, Y.Z. Jin, P.C.P. Watts, Growing multihydroxyl hyperbranched polymers on the surfaces of carbon nanotubes by in situ ring-opening polymerization, Macromolecules 37 (2004) 8846–8853.
[28] C. Gao, C.D. Vo, Y.Z. Jin, W.W. Li, S.P. Armes, Multihydroxy polymer-functionalized carbon nanotubes: synthesis, derivatization, and metal loading, Macromolecules 38 (2005) 8634–8648.
[29] H. Kong, C. Gao, D.Y. Yan, Controlled functionalization of multiwalled carbon nanotubes by in situ atom transfer radical polymerization, J. Am. Chem. Soc. 126 (2004) 412–413.
[30] K.C. Park, T. Hayashi, H. Tomiyasu, M. Endo, M.S. Dresselhaus, Progressive and invasive functionalization of carbon nanotube sidewalls by diluted nitric acid under supercritical conditions, J. Mater. Chem. 15 (2005) 407–411.
[31] J.L. Bahr, J.M. Tour, Covalent chemistry of single-wall carbon nanotubes, J. Mater. Chem. 12 (2002) 1952–1958.
[32] F. Liu, X.B. Zhang, J.P. Cheng, J.P. Tu, F.Z. Kong, W.Z. Huang, C.P. Chen, Preparation of short carbon nanotubes by mechanical ball milling and their hydrogen adsorption behavior, Carbon 41 (2003) 2527–2532.
[33] A. Hirsch, Functionalization of single-walled carbon nanotubes, Angew. Chem. Int. Ed. 41 (2002) 1853–1859.
[34] J. Kastner, T. Pichler, H. Kuzmany, S. Curran, W. Blau, D.N. Weldon, M. Delamesiere, S. Draper, H. Zandbergen, Fullerene pipes, Science 280 (1998) 1253–1256.
[35] J. Kastner, T. Pichler, H. Kuzmany, S. Curran, W. Blau, D.N. Weldon, M. Delamesiere, S. Draper, H. Zandbergen, Resonance Raman and infrared spectroscopy of carbon nanotubes, Chem. Phys. Lett. 221 (1994) 53–58.
[36] J. Peng, X. Qu, G. Wei, J. Li, J. Qiao, The cutting of MWNTs using gamma radiation in the presence of dilute sulfuric acid, Carbon 42 (2004) 2741–2744.
[37] B.H. Stuart, Infrared Spectroscopy: Fundamentals and Applications, John Wiley and Sons Ltd., Chichester, 2004.
[38] J.P. Hu, J.H. Shi, S.P. Li, Y.J. Qin, Z.X. Guo, Y.L. Song, D.B. Zhu, Red-emitting cerium-based phosphor materials for solid-state lighting applications, Chem. Phys. Lett. 401 (2005) 352–356.
[39] M.R. McPhail, J.A. Sells, Z. He, C.C. Chusuei, Charging nanowalls: adjusting the carbon nanotube isoelectric point via surface functionalization, J. Phys. Chem. C 113 (2009) 14102–14109.
[40] N.P. Blanchard, R.A. Hatton, S.R.P. Silma, Tuning the work function of surface oxidized multi-wall carbon nanotubes via cation exchange, Chem. Phys. Lett. 434 (2007) 92–95.
[41] Y. Xing, L. Li, C.C. Chusuei, R.V. Hull, Sonochemical oxidation of multiwalled carbon nanotubes, Langmuir 21 (2005) 4185–4190.
[42] C.Y. Yen, Y.F. Lin, C.H. Hung, Y.H. Tseng, C.C. Ma, M.C. Chang, H. Shao, The effects of synthesis procedures on the morphology and photocatalytic activity of multi-walled carbon nanotubes/TiO_2 nanocomposites, Nanotechnology 19 (2008) 045604.
[43] I. Farbman, S. Efrima, Studies of the structure of silver metal liquid-like films by UV–visible reflectance spectroscopy, J. Phys. Chem. 96 (1992) 8469–8473.
[44] B.H. Xia, H.X. Zhang, C.M. Che, K.H. Leung, D.L. Phillips, N. Zhu, Z.Y. Zhou, Metal-metal interactions in heterobimetallic d8-d10 complexes. structures and spectroscopic investigation of $[M'M''(\text{-dcpm})2(CN)2]^+$ (M' = Pt, Pd; M'' = Cu, Ag, Au) and related complexes by UV–vis absorption and resonance Raman spectroscopy and ab initio calculations, J. Am. Chem. Soc. 125 (2003) 10362–10374.
[45] K. Shimizu, K. Sugino, K. Kato, S. Yokota, K. Okumura, A. Satsuma, Formation and redispersion of silver clusters in Ag-MFI zeolite as investigated by time-resolved QXAFS and UV–Vis, J. Phys. Chem. C 111 (2007) 1683–1688.
[46] A. Pyatenko, M. Yamaguchi, M. Suzuki, Synthesis of spherical silver nanoparticles with controllable sizes in aqueous solutions, J. Phys. Chem. C 111 (2007) 7910–7917.
[47] Z.H. Mbhele, M.G. Salemane, C.G. vanSittert, J.M. Nedeljkovic, V. Djokovic, A.S. Luyt, Fabrication and characterization of silver-polyvinyl alcohol nanocomposites, Chem. Mater. 15 (2003) 5019–5024.
[48] R.W. Sun, R. Chen, N.P. Chung, C.M. Ho, C.L. Lin, C.M. Che, Silver nanoparticles fabricated in Hepes buffer exhibit cytoprotective activities toward HIV-1 infected cells, Chem. Commun. 40 (2005) 5059–5061.
[49] M. Kawashita, S. Tsuneyama, F. Miyaji, T. Kokubo, H. Kozuka, K. Yamamoto, Antibacterial silver-containing silica glass prepared by sol–gel method, Biomaterials 21 (2000) 393–398.
[50] H.J. Jeon, S.C. Yi, S.G. Oh, Preparation and antibacterial effects of Ag–SiO_2 thin films by sol–gel method, Biomaterials 24 (2003) 4921–4928.
[51] R. Kumar, H. Munstedt, Silver ion release from antimicrobial polyamide/silver composites, Biomaterials 26 (2005) 2081–2088.
[52] R. Krupke, F. Hennrich, O. Hampe, M.M. Kappes, Near-infrared absorbance of single-walled carbon nanotubes dispersed in dimethylformamide, J. Phys. Chem. B 107 (2003) 5667–5669.
[53] M.E. Itkis, D.E. Perea, S. Niyogi, J. Love, J. Tang, A. Yu, C. Kang, R. Jung, R.C. Haddon, Optimization of the Ni–Y catalyst composition in bulk electric zrc synthesis of single-walled carbon nanotubes by use of near-infrared spectroscopy, J. Phys. Chem. B 108 (2004) 12770–12775.
[54] K. Sbai, A. Rahmani, H. Chadli, Infrared spectroscopy of single-walled carbon nanotubes, J. Phys. Chem. B 110 (2006) 12388–12393.
[55] T.S. Wu, K.X. Wang, G.D. Li, S.Y. Sun, J. Sun, J.S. Chen, Montmorillonite-supported Ag/TiO_2 nanoparticles: an efficient visible-light bacteria photodegradation material, ACS Appl. Mater. Interfaces 2 (2010) 544–550.